COMMUNICATIONS IN SCIENCE AND TECHNOLOGY
Homepage: cst.kipmi.or.id

Effect of layered double hydroxide-graphene oxide modifier composition on characteristics of polyvinylidene fluoride based nanocomposite membranes in the separation of Cu^{2+}

Nita Kusumawati[a], Pirim Setiarso[a,*], Supari Muslim[b], Sinta Anjas Cahyani[a], Nafisatus Zakiyah[a], Ashabul Kahfi[a]

[a]*Department of Chemistry, Universitas Negeri Surabaya, Surabaya 60231, Indonesia*
[b]*Department of Electrical Engineering, Universitas Negeri Surabaya, Surabaya 60231, Indonesia*

Article history:
Received: 24 May 2024 / Received in revised form: 17 June 2024 / Accepted: 19 June 2024

Abstract

This research explored the modified polyvinylidene fluoride (PVDF) nanofiber membranes with a composite of layered double hydroxide (LDH) and graphene oxide (GO) to enhance biofouling resistance. The PVDF/LDH-GO nanocomposite membranes were synthesized via vacuum filtration. FTIR analysis confirmed nanocomposite formation with new peaks indicating the presence of GO and LDH. Variations in the LDH:GO ratio affected the physical, mechanical, and performance properties of the membranes. Based on SEM imaging, the 1:1 LDH: GO ratio exhibited the highest Young's modulus and smallest pore sizes. LDH-GO incorporation increased the mechanical strength, porosity, roughness, hydrophilicity, and pure water permeability of the PVDF membranes. The combination of these factors led to balanced permeability and selectivity values towards Cu^{2+} solution feeds. LDH-GO was proven effective in modifying the PVDF membrane surface for water treatment and inhibiting biofouling up to 64% against E. coli.

Keywords: LDH, GO, nanocomposite, PVDF, water treatment

1. Introduction

The growth of the world population and the acceleration of industrialization are the significant contributors to the increasing water pollution problems [1]. This condition triggers serious contamination of ground and surface water, thereby impacting the survival of various ecosystems and environmental vitality [2]. To overcome this, the use of membrane technology has become commonplace due to its superior performance and simple operation [3]. However, advances in membrane technology still require concentrated efforts to achieve several superior characteristics, such as high and balanced permeability and selectivity, resistance to various contaminants, and chemical resistance during the water treatment process [4,5]. For this, several researchers have engineered composite membranes using modification approaches, including grafting, layer-by-layer self-assembly, and blending [6,7].

Polyvinylidene fluoride (PVDF) is widely used as a membrane polymer material because of its extraordinary thermal, chemical, and mechanical resistance, as well as its ability to form asymmetric membranes [8]. However, its practical application is hampered by its extreme hydrophobic characteristics that cause fouling. This condition is exacerbated by the deposition and proliferation of microorganisms (biofouling) [9,10,11]. In this regard, hydrophilic and antibacterial modifications have emerged as the promising methods for controlling fouling and biofouling [12,13].

Graphene oxide (GO) is recognized as a potential modifier for its mechanical and thermal stability, hydrophilic properties, and ability as a versatile grafting material with various special functions [14]. Even though it has many superior properties, including antibacterial activity, its blending with polymers is reported to greatly reduce these advantages [15]. Therefore, in this study, the use of GO was more directed as a graft carrier for other hydrophilic and anti-bacterial agents to increase the flux and reduce the extreme biofouling of the PVDF membrane.

Layered double hydroxide (LDH) or $[M^{2+}1\text{-}XM^{3+}(OH)_2](An^-)x/n.mH_2O$, is a two-dimensional material characterized by a positively charged host layer and negatively charged insert ions [16]. It has anionic clay properties with a positively charged layered structure and a hydroxide-like

* Corresponding author.
Email: pirimsetiarso@unesa.ac.id
https://doi.org/10.21924/cst.9.1.2024.1440

composition, as well as antibacterial activity, which makes it not only as a hydrophilic and antibacterial agent but also as a favorable intercalation agent when combined with GO [15]. The simple synthesis method, cost-effectiveness, and efficacy in absorbing dyes and heavy metals make the use of LDH as a PVDF membrane modifier increasingly promising [17,18].

To obtain better LDH stability on PVDF membranes, in this study electrostatic grafting was carried out through carboxyl groups and GO epoxy as active sites for chemical modification using vacuum filtration, resulting in an LDH/GO modifier layer. The success of LDH-GO grafting on PVDF membrane was evaluated using Fourier Transform Infrared (FTIR). The varying compositions of PVDF/LDH-GO were evaluated to obtain membranes with the best mechanical characteristics and performance in Cu^{2+} separation. Here, the analysis of the mechanical resistance, wetting behavior, and performance of the membrane was expected to reflect the main impact of the LDH-GO modifier in improving the quality of the pore structure and effectiveness in producing comparable and high permeability and selectivity as a consequence of increasing the hydrophilic properties and porosity of the PVDF/LDH-GO membrane. Membranes with superior qualifications were characterized using atomic force microscopy (AFM) to see a decrease in the hydrophobicity of the PVDF membrane after modification using LDH-GO.

2. Materials and Methods

2.1. Materials

Several materials used include: Poly(vinylidene fluoride) (PVDF) (powder, Mw~534,000; Sigma-Aldrich, France), DMAc (N,N-Dimethylacetamide) (≥99.8%; Merck, Germany); HCl (≥37%; Fluka, Austria), H_2O_2 (30%; Smart-Lab, Indonesia), $NaNO_3$ (99%; Smart-Lab, Indonesia), H_2SO_4 (98%), $KMnO_4$ (≥99%, Merck, Singapore), $Mg(NO_3)_2.6H_2O$ (for analysis; Merck, Germany), $CuSO_4$ (anhydrous; ≥99.99%; Merck, Singapore), NaOH (Pellet; ≥98%; Merck, Germany), Na_2CO_3 (≥99.5%; Smart-Lab, Indonesia); graphite (powder; extra pure; Merck, Germany), and $Al(NO_3)_3.9H_2O$ (for analysis; Merck, Germany); and distilled water (CV. Chemical Indonesia Multi Sentosa, Indonesia).

2.2. Method

2.2.1. PVDF membrane preparation

The electrospinning method was used to create PVDF membranes. A solution of PVDF 18% (w/v) was dissolved in a combination of acetone and N, N-dimethylacetamide (DMAc) in a 2:3 ratio. To ensure the homogeneity of the polymer solution, stirring was carried out at 65°C with a speed of 270 rpm for 12 hours. The electrospinning process was carried out using a voltage of 15 kV, a flow rate of 1 mL/hour, and a distance between the injector and collector drum of 15 cm.

2.2.2. Preparation of LDH, GO, and LDH/GO composite system

Mg-Al LDH production was carried out using the direct coprecipitation method, following the procedure of Zeng et al. [19]. The aqueous mixture of $Al(NO_3)_3.9H_2O$ and $Mg(NO_3)_2.6H_2O$ with a molar ratio of 1:2 in 100 mL of deionized water was rapidly stirred at 65°C. Simultaneously, a mixture of 2.0 M NaOH and 0.5 M Na_2CO_3 was added to maintain a pH of 9-10. After aging for 18 hours, the colloid mixture was centrifuged at a speed of 8000 rpm for 10 minutes. The resulting precipitate was washed repeatedly with distilled water until obtaining a neutral pH. The precipitate was dried overnight at 85°C.

GO was synthesized by modifying the Hummers and Offerman procedure [20]. Specifically, 230 mL of cold sulfuric acid was added into a mixture of 10 grams of graphite and 5 grams of $NaNO_3$, accompanied by gradual stirring at 10°C. 30 grams of $KMnO_4$ were then added. The mixture was stirred for 30 minutes and heated at 35°C. After adding 250 mL of distilled water, the heat was raised to 90°C, and the stirring was maintained for 30 minutes. To reduce excess KMnO4, 500 mL of distilled water and 50 mL of H2O2 (30%v/v) were added to stop the oxidation reaction. The resulted sample then underwent centrifugation at 8000 rpm for 10 minutes. The dried precipitate was obtained by subjecting it to a vacuum oven at 60°C for 24 hours.

The resulting LDH and GO powders were dispersed in 100 mL of distilled water at a speed of 300 rpm for 1 hour with variations as shown in Table 1. The LDH/GO solution was ultrasonicated for 30 minutes to obtain a composite, which was ready to be processed in the next stage.

Table 1. Mass ratio of LDH/GO in the PVDF composite membrane

Sample	M0	M1	M2	M3	M4	M5	M6	M7	M8	M9
LDH (mg)	0	20	20	20	20	20	15	10	5	0
GO (mg)	0	0	5	10	15	20	20	20	20	20

2.2.3. Membrane preparation

The PVDF membrane (d 6 cm) was immersed in a mixture of ethanol-distilled water for 5 min. It was then modified through a vacuum filtration process using 50 mL of LDH/GO solution (M0-M9) to obtain a PVDF/LDH-GO composite membrane.

2.3. Characterization of membrane

The successful formation of the PVDF/LDH-GO composite membrane was confirmed using the Perkin Elmer Fourier Transform Infrared (FTIR) Spectrum Two. The mechanical resistance of the membrane was evaluated using the RCT-10KN-AF Toyo Seiki Strograph. The surface and cross-section morphology of the membrane were observed using the FEI Inspect S50 Scanning Electron Microscope (SEM), while the description of changes in the membrane porosity before and after modification using LDH-GO were observed based on the changes in membrane roughness as a result of analysis using

Bruker Atomic Force Microscopy (AFM). Membrane performance was determined using a "Dead-end" membrane reactor (homemade). The permeate produced from this stage was analyzed using Shimadzu Atomic Absorption Spectrophotometry (AAS) AA-7000 to obtain membrane selectivity.

2.4. Membrane porosity analysis

The porosity can be calculated by analyzing the SEM image using the OriginPro 2018 software. The parameters to determine the porosity of the sample include the values of Hmax, Hmin, X, Y, integral volume, total volume, solid volume, volume under the curve, pore volume, and porosity percentage [21,22]. The porosity calculation in the software is in accordance to the equation:

$$V_{solid} = \int_{x_{min}}^{x_{max}} \int_{y_{min}}^{y_{max}} f\,(x,y)dxdy \quad (1)$$

where X_{max}, X_{min}, Y_{max}, Y_{min} are the surface boundaries at X and Y coordinates (surface boundaries when projected on the base plane) with X_{max}. Specifically, equation 2 is used to find the total volume.

$$V_{total} = f_{max}\,(\mathrm{x}_{max} - \mathrm{x}_{min})(\mathrm{y}_{max} - \mathrm{y}_{min}) \quad (2)$$

The difference between total volume and solid volume was used to find the pore volume, while to calculate porosity and its percentage, equation 3 was used.

$$\phi = \frac{V_p}{V_{tot}} \quad (3)$$

where ϕ is porosity, V_p is pore volume, and V_{tot} is total volume.

2.5. Performance evaluation of membranes

The permeability and selectivity of the PVDF/LDH-GO membrane were calculated using Equations 1 & 2:

$$\mathrm{J} = \frac{V}{A \times t} \quad (4)$$

$$\mathrm{R} = \left(1 - \frac{C_p}{C_f}\right) \times 100\% \quad (5)$$

J represents the pure water flux and is measured in $Lm^{-2}h^{-1}$. V stands for the permeation volume and is expressed in liters. A denotes the effective membrane area in square meters (m^2) and t is the filtration time and is measured in hours. R represents the Cu^{2+} removal ratio and is expressed as a percentage. Meanwhile, C_f and C_p are the concentrations of Cu^{2+} in the feed and permeate, respectively.

2.6. Antibacterial performance of membrane

To determine the effect of LDH-GO modification on the risk of biofouling, the membrane's inhibition ability on bacterial growth was evaluated using the agar disc diffusion method. Escherichia coli was chosen to represent gram-negative bacteria. Before culturing on Mueller-Hinton agar plates, each bacterial sample was introduced into a suspension with an approximate concentration of 1.5 × 108 colony-forming units per milliliter (cfu/mL). The 12 mm diameter PVDF/LDH-GO membrane was incubated at 37°C for 24 hours. Three areas of inhibition zone measurement were determined using a caliper. The presence of an inhibition zone on each membrane was used to measure the antibacterial activity of the PVDF/LDH-GO composite membrane [23].

3. Results and Discussion

3.1. Membrane characterization

3.1.1. Chemical characterization

Fig. 1 shows the comparison of the IR spectra of PVDF/LDH-GO (M0-M9) membranes. The pure PVDF membrane (M0) showed a peak at 1401.51 cm^{-1}, indicating C-H stretching and deformation. The presence of the C-F group was indicated by the appearance of a peak at 1171.32 cm^{-1}. The peak at 876.07 cm^{-1} indicated the PVDF β-phase [9,19,24,25]. All three were also detected on M1-M9. In contrast to M0, the IR spectrum of M1-M9 showed a distinctive peak at 2959.49-3020.36 cm^{-1} as a marker of the presence of the O-H group as the main feature of GO. This peak was visible in the IR spectrum of M4. In this spectrum, a typical C=O peak at 1732.84 cm^{-1} was also observed, which further confirmed the presence of GO in the composite membrane. The lower GO composition in the M1-M3 modifier composition made the appearance of the typical peak of this group less observed. Meanwhile, the undetectable appearance of this group in the IR spectrum of M5 was assumed to be closely related to the optimal intercalation of LDH in the GO layer of the composite membrane. Interestingly, despite having the similar GO content as M5, the C=O peak was also present in the M6-M9 samples, albeit with varying intensities. This variation in peak intensity across M6-M9 could be attributed to differences in the extent of LDH-GO interactions and the degree of GO functionalization, which might determine the visibility of the C=O stretching vibration in the FTIR spectra. The presence of LDH in the composite membrane was detected from the appearance of a peak at 595.10-601.68 cm^{-1}. This peak indicated the stretching vibrations of O-M-O, M-O, and M-O-M, where M represents Al and Mg, as reported by Zeng et al [19]. The overall interpretation of this IR spectrum showed the successful formation of the PVDF/LDH-GO composite membrane.

3.1.2. Mechanical characterization

The PVDF/LDH-GO membrane's mechanical strength was assessed using Young's modulus, which was computed through Equation 6.

$$\mathrm{E} = \frac{strees}{strain} \quad (6)$$

Increasing the LDH mass in the LDH-GO modifier caused an increase in the quantity of LDH nanoparticles deposited on the membrane surface, which then manifested as LDH clusters.

LDH distributed between the GO sheets through the pores of the PVDF membrane and formed pores between the sheets. By comparing the M6-M9 data, a significant increase in the Young's modulus value was observed as the LDH mass increased. The same pattern was also observed as the GO mass increased. The increase in GO layers then created a more stable framework for LDH intercalation [26]. This was what made the increase in Young's modulus due to the increasing GO levels slightly higher than LDH. Young's modulus reached the maximum when the mass ratio of LDH was 20 mg and GO was 20 mg in the modifier, as in M5. Increasing the quantity of GO layers and the amount of LDH intercalation in the GO layer on the membrane surface simultaneously increased the ability of the PVDF/LDH-GO composite membrane to maintain pore size when exposed to pressure.

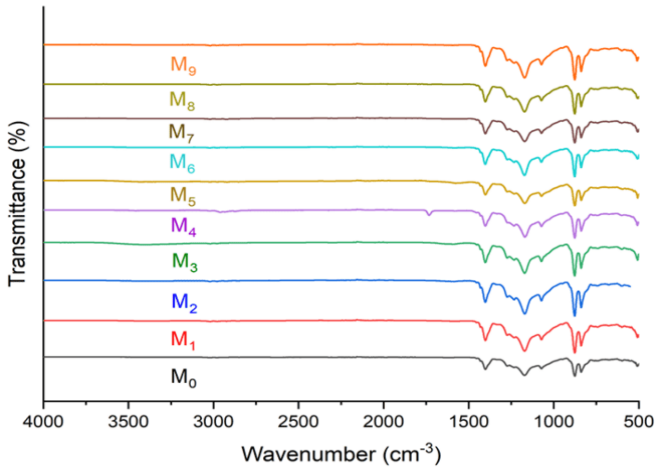

Fig. 1. Infra-red spectra of PVDF and PVDF/LDH-GO membranes

3.1.3. Mechanical characterization

The PVDF/LDH-GO membrane's mechanical strength was assessed using Young's modulus, which was computed through Equation 6.

$$E = \frac{strees}{strain} \quad (6)$$

Increasing the LDH mass in the LDH-GO modifier caused an increase in the quantity of LDH nanoparticles deposited on the membrane surface, which then manifested as LDH clusters. LDH distributed between the GO sheets through the pores of the PVDF membrane and formed pores between the sheets. By comparing the M6-M9 data, a significant increase in the Young's modulus value was observed as the LDH mass increased. The same pattern was also observed as the GO mass increased. The increase in GO layers then created a more stable framework for LDH intercalation [26]. This was what made the increase in Young's modulus due to the increasing GO levels slightly higher than LDH. Young's modulus reached the maximum when the mass ratio of LDH was 20 mg and GO was 20 mg in the modifier, as in M5. Increasing the quantity of GO layers and the amount of LDH intercalation in the GO layer on the membrane surface simultaneously increased the ability of the PVDF/LDH-GO composite membrane to maintain pore size when exposed to pressure.

Table 2. Young's Modulus of PVDF and PVDF/LDH-GO Membranes

Code	Membrane	LDH composite (mg)	GO composite (mg)	Young's Modulus (MPa)
M0	PVDF	0	0	0.998
M1	PVDF	20	0	1.051
M2	PVDF	20	5	1.117
M3	PVDF	20	10	1.134
M4	PVDF	20	15	1.142
M5	PVDF	20	20	1.239
M6	PVDF	15	20	1.139
M7	PVDF	10	20	1.091
M8	PVDF	5	20	1.045
M9	PVDF	0	20	1.005

3.1.4. Physical characterization

Fig. 2 shows the surface morphology and cross-section of the PVDF/LDH-GO membrane. Fig. 2(a) shows a smooth surface with large pores on the PVDF membrane. Fig. 2 (b and d) shows a decrease in pore dimensions and an increase in the porosity at the same time as the GO mass increased. In line with this, Fig. 2 (d and f) shows an increase in the porosity and a decrease in pore dimensions as the LDH mass increased. Increasing the mass of GO and LDH resulted in the production of a GO layer in the pore dimensions of the PVDF membrane and LDH nanoparticles intercalated between the GO sheets, forming an internal pore layer. Fig. 3 shows the cross-sectional morphology of the PVDF and PVDF/LDH-GO membranes, which overall had an asymmetric structure. The combination of the LDH-GO modifier on the PVDF membrane produced a smaller pore size, both in the skin layer and in micropores (sponge- and finger-like pore), as seen in the M5 membrane as observed to have the smallest pore dimensions.

The increase in grafted GO layers provided stronger structural support, while the increase in deposition of LDH nanoparticles in the gaps between GO sheets resulted in a tighter pore structure. The mechanical resistance of PVDF membranes was improved by the combined action of both mechanisms produced by this LDH-GO modifier, resulting in higher Young's modulus values [27,28].

Electrostatic interactions were formed between the negative charge of GO and the positive charge of the LDH surface, facilitated by the carboxyl group. This interaction effectively prevented the re-stacking of GO nanosheets, resulting in the formation of an intercalated membrane with a smaller pore size. This observation is in line with several studies reporting the important role of electrostatic interactions in preventing the re-stacking of GO nanosheets and the formation of intercalation membranes [18,19].

Even though there was a decrease in the pore size of the PVDF membrane, the SEM images could not show changes in porosity occurred when the LDH-GO modifier was grafted. OriginPro 2018 software was used to calculate membrane porosity based on SEM images. The values obtained from this application included Hmax, Hmin, X, Y, and integral volume

[22,23]. These five were used to calculate total volume, solid volume, volume under the curve, pore volume, and membrane porosity percentage. Equation 1 was used to get the solid volume, while Equation 2 was used to get the total volume. The percentage of porosity was calculated from the difference between total volume and solid volume (see Equation 3). Porosity was depicted using a 3D graph, as shown in Fig. 4, and quantified, as shown in Table 3.

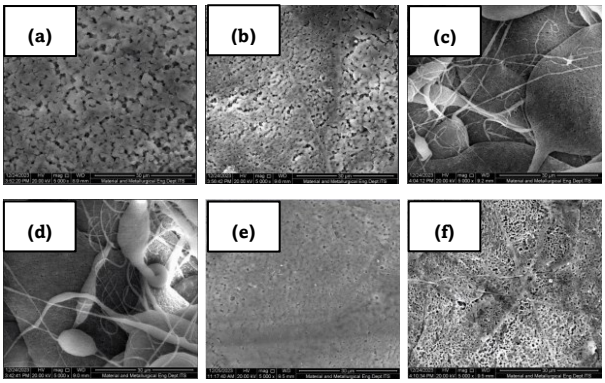

Fig. 2. SEM results of membrane surface morphology: (a) M0, (b) M1, (c) M3, (d) M5, (e) M7, and (f) M9

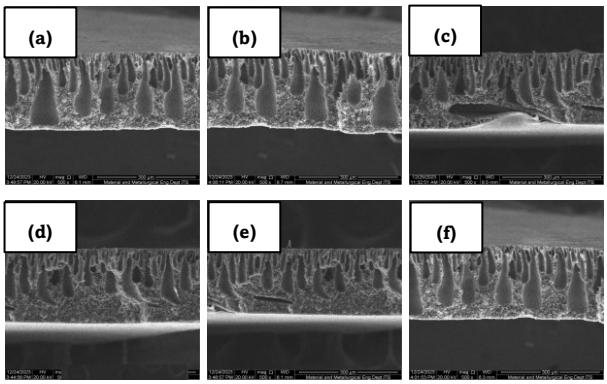

Fig. 3. SEM results of membrane cross-section morphology: (a) M0, (b) M1, (c) M3, (d) M5, (e) M7, and (f) M9

These results indicated that the LDH-GO grafting modifier caused an increase in porosity in the PVDF membrane. The vacuum filtration process has allowed GO to fill membrane pores and created a new pore framework, which was then sealed by the intercalation of LDH in each GO layer. Thus, the electrostatic interaction of the two in the internal pores of the PVDF membrane produced many new pores with higher pore density. This fact was reinforced by the acquisition of the highest porosity percentage by M5. Specifically, the increase in porosity occurred with increasing GO was found slightly higher than that of LDH. The intercalation of LDH in each GO layer should create more new small spaces in the internal pores of the PVDF membrane compared to GO, which tended to create large open spaces. This was predicted to be related to the non-optimal intercalation of LDH in the GO layer.

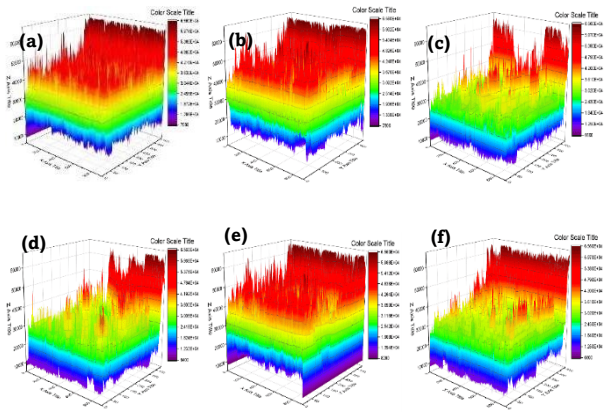

Fig. 4. 3D porosity graph of the: (a) M0, (b) M1, (c) M3, (d) M5, (e) M7, and (f) M9

Table 3. Membrane Porosity

Code	Membrane	LDH composite (mg)	GO composite (mg)	Porosity (%)
M0	PVDF	0	0	65.06
M1	PVDF	20	0	66.57
M3	PVDF	20	10	72.83
M5	PVDF	20	20	74.89
M7	PVDF	10	20	72.24
M9	PVDF	0	20	66.74

Apart from calculations using OriginPro 2018 software, the increase in membrane porosity was also evaluated using AFM. Fig. 5 respectively shows 3D images of the AFM surfaces M0 and M5 along with the values of their surface roughness parameters, average roughness (Ra) and root mean square roughness (Rq). The results showed that the PVDF membrane in its pure form (M0) boasted the smoothest surface with an average roughness (Ra) measuring at 62.4 nm and a root mean square roughness (Rq) measuring at 77.6 nm. Conversely, M5 exhibited a notable increase in surface roughness with a Ra measuring at 92.8 nm and a (Rq) measuring at 118 nm, when compared to M0. Increasing surface roughness tended to increase the filtration area, thereby triggering an increase in membrane flux, as illustrated by the permeability values of pure water and Cu^{2+} (see Fig. 5).

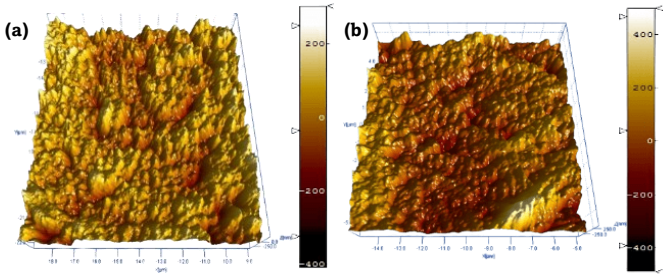

Fig. 5. The surface roughness of (a) M0; and (b) M5

3.2. Wetting behavior

Pure water permeability measurements were used to confirm the enhanced hydrophilic characteristics of the composite membrane when the LDH-GO modifier was present. In addition to increasing the flux, the increase in hydrophilic characteristics could help the formation of a water layer over the membrane. This layer functioned as a protective barrier, blocking contaminants from directly contacting the membrane surface. Thus, increased hydrophilic properties resulted in greater resistance to membrane fouling/biofouling [7,29]. Fig. 6 shows the pure water flux produced by M0-M9. Two similar increasing patterns are shown as GO mass (M0-M4) and LDH mass (M9-M6) increase. The highest pure water permeability was produced by M5, where the masses of GO and LDH in the modifier composition were the most abundant and balanced. The pattern of increasing pure water flux, corresponding to the increasing mass of GO and LDH, was related to the rising hydrophilic characteristics of the membrane. The presence of hydroxyl groups (-OH) on the LDH surface resulted in an increase in the interlayer distance in graphene oxide (GO), which resulted in a greater penetration rate of water molecules in the nanocomposite membrane [30,31]. Not only did it improve the distance between GO sheets and change the pore structure through intercalation which triggers the expansion of water penetration channels, LDH also increased the hydrophilic properties of the membrane and reduced its resistance to water penetration [32].

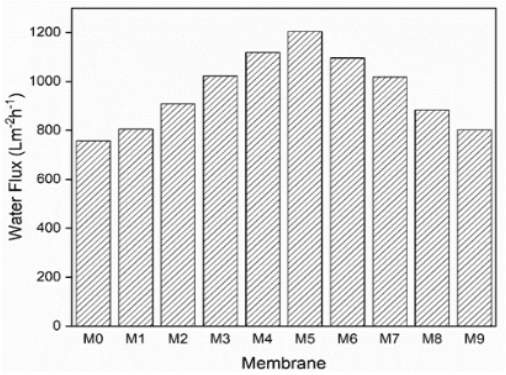

Fig. 6. Water flux data of the membrane

Table 4. Antibacterial activity of PVDF and PVDF/LDH-GO Membranes

Code	Membrane	LDH composite (mg)	GO composite (mg)	Inhibitory Zone (mm)
M0	PVDF	0	0	8.32
M1	PVDF	20	0	9.52
M2	PVDF	20	5	10.38
M3	PVDF	20	10	11.80
M4	PVDF	20	15	13.08
M5	PVDF	20	20	13.65
M6	PVDF	15	20	13.47
M7	PVDF	10	20	12.40
M8	PVDF	5	20	11.32
M9	PVDF	0	20	9.85

3.3. Performance

Fig. 7 illustrates the flux and rejection rate of Cu^{2+} of various membranes (M0–M9). The LDH-GO PVDF membrane's permeability and selectivity towards Cu^{2+} were assessed using a $CuSO_4$ solution. The increase in LDH mass in the modifier composition triggered an increase in flux from 835.67 $Lm^{-2}h^{-1}$ (M9) to 1146.50 $Lm^{-2}h^{-1}$ (M6). The same pattern of increasing flux was also found with the increasing GO mass in the modifier. The hydrophilic nature of LDH and the expansion of the distance between GO layers due to LDH intercalation, which caused increasing porosity were predicted to be the triggers. This is in line with what was reported by Jana et al. [33]. The highest flux was produced by M5 where the mass ratio of LDH and GO was balanced.

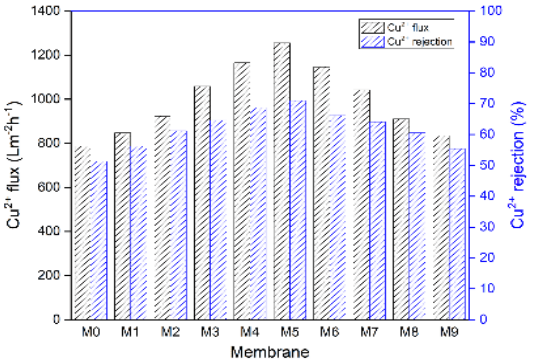

Fig. 7. Cu^{2+} flux and rejection of PVDF/LDH-GO membrane

The PVDF membrane with pure LDH modifier (M1) had a 5.85% lower flux than the one with pure GO modifier (M9). The existence of multilayer GO was the background for this superiority. However, the combination of both (LDH and GO) as modifiers could optimize the performance of nanocomposite membranes in removing Cu^{2+}. First, the presence of LDH intercalation would increase porosity accompanied by a decrease in pore size. This condition allowed the acquisition of flux and rejection that were comparable. This could be proven by the flux and rejection of Cu^{2+} from M6, which were both higher than M9. Furthermore, the presence of hydroxyl groups on the surface of LDH, which formed a chelate with Cu^{2+} further increased the rejection effect. Cu^{2+} adsorbed on LDH via ion exchange and surface complexation, but mainly by surface complexation. This is in line with what was published by Awes et al. dan Hu et al. [17,34]. Second, without the presence of LDH, GO in the modifier tended to experience complexation with Cu^{2+} during filtration. This condition then would cause a reduction in the distance between GO layers, resulting in lower flux [34].

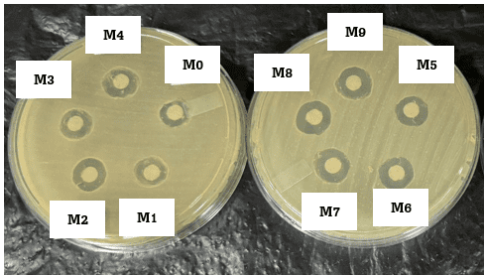

Fig. 8. Inhibitory zone of the membrane

3.4. Antibacterial performance of membrane

As shown in Table 4, to obtain the benefits of the LDH-GO grafting modifier in reducing the risk of biofouling, the antibacterial activity of the PVDF/LDH-GO membrane against Escherichia coli (E. coli) was evaluated based on the diameter of the inhibition zone of the suspension on each membrane. The results of testing the antibacterial activity of E. coli showed the highest results in M5.

The successful grafting of the LDH-GO modifier has resulted in an obvious inhibition zone around the PVDF/LDH-GO membrane sample. The diameter of this inhibition zone increased as the mass of GO in the modifier increased. This was due to the multiple antibacterial mechanisms of GO, which included oxidative and membrane stress, entrapment, photothermal effects, and basal planes. Additionally, the pointed edges of graphene oxide nanosheets had the potential to physically damage bacterial membranes, causing bacterial inactivation and intracellular matrix leakage. In addition, barriers to gas/ion exchange prevented bacteria from multiplying as they were isolated from their environment. This marked the point at which bacteria became immobile on the composite GO sheet [36]. In line with this, an increase in the diameter of the inhibition zone was detected, which was even higher compared to GO, as the mass of LDH in the modifier grafted on the membrane increased. The interaction of GO on two sides, namely with the PVDF membrane and the LDH modifier, reduced the reactivity of its functional groups towards bacteria. On the other hand, the attachment and absorption of bacteria to the surface of the LDH modifier through electrostatic forces increased antibacterial effectiveness [37].

4. Conclusion

Membrane modification using LDH-GO modifier was found capable of improving both the physical and mechanical characteristics and performance of PVDF membranes in Cu^{2+} separation. The use of GO as the sole modifier material produced the flux values of pure water and Cu^{2+} which were far below the membrane flux with the LDH-GO combination modifier. LDH's ability to form intercalations and increase the distance between GO layers was able to improve the pore structure (increasing porosity and decreasing pore size), which not only resulted in increasing mechanical resistance but also membrane permeability (>53.10% for pure water; and 53.35 % for Cu^{2+}). At the same time, an increase in the Cu^{2+} rejection percentage was also detected, reaching 71% for M5. The use of GO as a carrier for the LDH antibacterial agent was proven to increase the antibacterial activity of PVDF membranes against *E. coli*. These collective findings showed a promising potential for utilizing the LDH-GO modifier, not only to suppress pore defects in PVDF membranes but also to increase its resistance to the risk of biofouling in water treatment applications.

Acknowledgment

The author would like to thank the Ministry of Education, Culture, Research and Technology of the Republic of Indonesia for the financial assistance provided.

Author Contributions: N.K.: conceptualization, methodology, formal analysis, writing original draft, review, and validation; P.S.: formal analysis, writing, review, and editing; S.M.: writing review and editing, analysis, and data curation;, S.A.C.: writing—review and editing, project administration, and validation; N.Z.: writing, investigation, resource, and review; A.K: writing review, editing, and project administration.. All authors have read and agreed to the published version of the manuscript.

Funding: This research was funded by the Ministry of Education, Culture, Research, and Technology of the Republic of Indonesia

Conflicts of Interest: The authors declare no conflict of interest

References

1. N. Maroufi, N. Hajilary, *Nanofiltration membranes types and application in water treatment: a review*, J. Sustain. Water Resour. Manag. 9 (2023) 1-18.
2. A.M. Pirzada, I. Ali, N.B. Mallah, G. Maitlo, *Development of novel PET-PAN electrospun nanocomposite membrane embedded with layered double hydroxides hybrid for efficient wastewater treatment*, Polymers 15 (2023) 4388.
3. N. Shehata, D. Egirani, A.G. Olabi, A. Inayat, M.A. Abdelkareem, K.-J. Chae et al., *Membrane-based water and wastewater treatment technologies: Issues, current trends, challenges, and role in achieving sustainable development goals, and circular economy*, Chemosphere 320 (2023) 137993.
4. N.H. Othman, N.H. Alias, N.S. Fuzil, F. Marpani, M.Z. Shahruddin, C.M. Chew et al., *A review on the use of membrane technology systems in developing countries*, Membranes 12 (2021) 30.
5. Y. Liu, M. Zhu, M. Chen, L. Ma, B. Yang, L. Li et al., *A polydopamine-modified reduced graphene oxide (RGO)/MOFs nanocomposite with fast rejection capacity for organic dye*, J. Chem. Eng. 359 (2019) 47-57.
6. M.R.S. Kebria, A. Rahimpour, G. Bakeri, R. Abedini, *Experimental and theoretical investigation of thin ZIF-8/chitosan coated layer on air gap membrane distillation performance of PVDF membrane*, Desalination 450 (2019) 21-32.
7. D. Zhang, F. Dai, P. Zhang, Z. An, Y. Zhao, L. Chen, *The photodegradation of methylene blue in water with PVDF/GO/ZnO composite membrane*, Mater. Sci. Eng. C 96 (2019) 684-692.
8. N. Kusumawati, P. Setiarso, A.B. Santoso, S. Muslim, Q. A'yun, M.M. Putri, *Characterization of poly(vinylidene fluoride) nanofiber-based electrolyte and its application to dye-sensitized solar cell with natural dyes*, Indones. J. Chem. 23 (2023) 113.
9. N. Kusumawati, P. Setiarso, S. Muslim, *Polysulfone/polyvinylidene fluoride composite membrane: Effect of coating dope composition on membrane characteristics and performance*, Rasayan J. Chem. 11 (2018) 1034-1041.
10. J.R. Mishra, S. Samal, S. Mohanty, S. Nayak, *Polyvinylidene fluoride (PVDF)/Ag@TiO2 nanocomposite membrane with enhanced fouling resistance and antibacterial performance*, Mater. Chem. Phys. 268 (2021) 124723.
11. W. Xie, J. Li, T. Sun, W. Shang, W. Dong, M. Li et al., *Hydrophilic modification and anti-fouling properties of PVDF membrane via in situ nano-particle blending*, Environ. Sci. Pollut. Res. 25 (2018) 25227-25242.
12. N. Kusumawati, P. Setiarso, M.M. Sianita, S. Muslim, *Transport*

properties, mechanical behavior, thermal and chemical resistance of asymmetric flat sheet membrane prepared from PSf/PVDF blended membrane on gauze supporting layer, Indones. J. Chem. 18 (2018) 257.

13. H. Zhang, S. Zhu, J. Yang, A. Ma, *Advancing strategies of biofouling control in water-treated polymeric membranes*, Polymers 14 (2022) 1167.
14. W. Wang, N. Zhang, Z. Ye, Z. Hong, M. Zhi, *Synthesis of 3D hierarchical porous Ni-Co layered double hydroxide/N-doped reduced graphene oxide composites for supercapacitor electrodes*, Inorg. Chem. Front. 6 (2019) 407-416.
15. X. Shen, P. Liu, S. Xia, J. Liu, R. Wang, H. Zhao et al., *Anti-fouling and anti-bacterial modification of poly(vinylidene fluoride) membrane by blending with the capsaicin-based copolymer*, Polymers 11 (2019) 323.
16. Y. Dong, C. Lin, S. Gao, N. Manoranjan, W. Li, W. Fang et al., *Single-layered GO/LDH hybrid nanoporous membranes with improved stability for salt and organic molecules rejection*, J. Membr. Sci. 607 (2020) 118184.
17. B. Hu, C. Huang, X. Li, G. Sheng, H. Li, X. Ren et al., *Macroscopic and spectroscopic insights into the mutual interaction of graphene oxide, Cu(II), and Mg/Al layered double hydroxides*, J. Chem. Eng. 313 (2017) 527-534.
18. E. Abdollahi, A. Heidari, T. Mohammadi, A.A. Asadi, M. Ahmadzadeh Tofighy, *Application of Mg-Al LDH nanoparticles to enhance flux, hydrophilicity and antifouling properties of PVDF ultrafiltration membrane: Experimental and modeling studies*, Sep. Purif. Technol. 257 (2021) 117931.
19. H. Zeng, Z. Yu, Y. Peng, L. Zhu, *Environmentally friendly electrostatically driven self-assembled PVDF/LDH-GO composite membrane for water treatment*, Appl. Clay Sci. 183 (2019) 105322.
20. W.S. Hummers, R.E. Offeman, *Preparation of graphitic oxide*, J. Am. Chem. Soc. 80 (1958) 1339-1349.
21. O. Brincoveanu, I.C. Marinas, P. Preda, *Determination of the average pore-size and porosity in collagen by image processing of SEM micrographs*, Int. Semicond. Conf. (2022).
22. R.F. Mushaddaq, A.A. Bama, Ramlan, T. Lestariningsih, *Elektrolit Polimer Padat dari Pencampuran PVDF-HFP dan PEO serta Modifikasi Filler Sebagai Bahan Dasar Baterai Lithium-Ion*, JST 12 (2023) 219-228.
23. X. Xu, Q. Wang, X. Zhu, Q. Wu, T. Zheng, H. Yuan et al., *The preparation of anti-fouling dual-layer composite membrane with embedding graphene oxide*, Asia-Pac. J. Chem. Eng. 18 (2023) e2949.
24. A. Islam, A.N. Khan, M.F. Shakir, K. Islam, *Strengthening of β polymorph in PVDF/FLG and PVDF/GO nanocomposites*, Mater. Res. Express 7 (2020) 015017.
25. X. Sun, H. Shiraz, R. Wong, J. Zhang, J. Liu, J. Lu et al., *Enhancing the performance of PVDF/GO ultrafiltration membrane via improving the dispersion of GO with homogeniser*, Membranes 12 (2022) 1268.
26. T. Xue, W. Fan, X. Zhang, X. Zhao, F. Yang, T. Liu, *Layered double hydroxide/graphene oxide synergistically enhanced polyimide aerogels for thermal insulation and fire-retardancy*, Compos. Part B Eng. 219 (2021) 108963.
27. M. Sajid, S.M. Sajid Jillani, N. Baig, K. Alhooshani, *Layered double hydroxide-modified membranes for water treatment: Recent advances and prospects*, Chemosphere 287 (2022) 132140.
28. Y. Cao, Z. Xiong, F. Xia, G.V. Franks, L. Zu, X. Wang et al., *New structural insights into densely assembled reduced graphene oxide membranes*, Adv. Funct. Mater. 32 (2022) 2201535.
29. S. Ayyaru, T.T.L. Dinh, Y.-H. Ahn, *Enhanced antifouling performance of PVDF ultrafiltration membrane by blending zinc oxide with support of graphene oxide nanoparticle*, Chemosphere 241 (2020) 125068.
30. N. Ghanbari, H. Ghafuri, *Preparation of novel Zn-Al layered double hydroxide composite as adsorbent for removal of organophosphorus insecticides from water*, Sci. Rep. 13 (2023) 10215.
31. H.-J. Qu, L.-J. Huang, Z.-Y. Han, Y.-X. Wang, Z.-J. Zhang, Y. Wang et al., *A review of graphene-oxide/metal-organic framework composites materials: characteristics, preparation and applications*, J. Porous Mater. 28 (2021) 1837-1865.
32. D. Makwana, V. Polisetti, J. Castaño, P. Ray, H.C. Bajaj, *Mg-Fe layered double hydroxide modified montmorillonite as hydrophilic nanofiller in polysulfone- polyvinylpyrrolidone blend ultrafiltration membranes: separation of oil-water mixture*, Appl. Clay Sci. 192 (2020) 105636.
33. A. Jana, O. Roy, S.S. Ravuru, S. De, *Tuning of graphene oxide intercalation in magnesium aluminium layered double hydroxide and their immobilization in polyacrylonitrile beads by single step mussel inspired phase inversion: A super adsorbent for lead*, J. Chem. Eng. 391 (2020) 123587.
34. H. Awes, Z. Zaki, S. Abbas, H. Dessoukii, A. Zaher, S.A. Abd-El Moaty et al., *Removal of Cu2+ metal ions from water using Mg-Fe layered double hydroxide and Mg-Fe LDH/5-(3-nitrophenyllazo)-6-aminouracil nanocomposite for enhancing adsorption properties*, Environ. Sci. Pollut. Res. 28 (2021) 47651-47667.
35. J. Li, Q. Huang, H. Yu, L. Yan, *Enhanced removal performance and mechanistic study of Cu2+, Cd2+, and Pb2+ by magnetic layered double hydroxide nanosheets assembled on graphene oxide*, J. Water Process Eng. 48 (2022) 102893.
36. P. Kumar, P. Huo, R. Zhang, B. Liu, *Antibacterial properties of graphene-based nanomaterials*, Nanomaterials 9 (2019) 737.
37. S.A.A. Abdel Aziz, Y. GadelHak, M.B.E.D. Mohamed, R. Mahmoud, *Antimicrobial properties of promising Zn-Fe based layered double hydroxides for the disinfection of real dairy wastewater effluents*, Sci. Rep. 13 (2023) 1-11.